

# PRECONDITIONED NONLINEAR CONJUGATE GRADIENT METHOD OF STRETCH ENERGY MINIMIZATION FOR AREA-PRESERVING PARAMETERIZATIONS\*

SHU-YUNG LIU<sup>†</sup> AND MEI-HENG YUEH<sup>†</sup>

**Abstract.** Stretch energy minimization (SEM) is widely recognized as one of the most effective approaches for the computation of area-preserving mappings. In this paper, we propose a novel preconditioned nonlinear conjugate gradient method for SEM with guaranteed theoretical convergence. Numerical experiments indicate that our new approach has significantly improved area-preserving accuracy and computational efficiency compared to another state-of-the-art algorithm. Furthermore, we present an application of surface registration to illustrate the practical utility of area-preserving mappings as parameterizations of surfaces.

**Key words.** nonlinear conjugate gradient method, simplicial surface, stretch energy minimization, simplicial mapping, area-preserving

**MSC codes.** 68U05, 65D18, 52C35, 33F05, 65E10

**1. Introduction.** An area-preserving parameterization, commonly called an authalic or equiareal parameterization, is a mapping on a surface that preserves the local area up to a global scaling factor. The factor is precisely the ratio between the total area of the surface and that of the specified target domain. Classical and state-of-the-art methods for area-preserving mapping include the stretch-minimizing method [15, 20], Lie advection method [27], optimal mass transportation method [6, 26, 18], diffusion-based method [5], and the stretch energy minimization (SEM) [25, 21]. Area-preserving mappings can be used as parameterizations and applied in tasks such as surface resampling, remeshing, and registration [8, 16, 9, 10, 13, 19, 24]. They can also serve as boundary parameterizations in image preprocessing for brain tumor segmentation [22, 23, 11, 12]. In particular, it has been demonstrated that the SEM approach [25] for numerical computing area-preserving mapping is more efficient and accurate in preserving the area than other state-of-the-art algorithms [20, 26]. Moreover, a recent study has established the equivalence between stretch energy minimizers and area-preserving mappings [21], further reinforcing the value of SEM in this context. The study also provides a neat explicit gradient formula of the stretch energy and the associated line-search gradient descent algorithm for computing a minimizer with guaranteed convergence. However, the gradient descent method slowly decreases the stretch energy, which is impractical for further application use. To remedy this drawback, we are motivated to develop an associated nonlinear conjugate gradient (CG) method to improve the efficiency of the SEM.

**1.1. Contribution.** In this paper, we propose a novel preconditioned nonlinear CG method of the SEM for the computation of area-preserving parameterizations of simply connected open surfaces. The contributions of this paper are as follows:

- (i) We rigorously prove the convergence of our proposed preconditioned nonlinear CG iteration of SEM for computing area-preserving parameterizations.
- (ii) Numerical comparisons with another state-of-the-art algorithm are demon-

---

\*Preprint submitted to arXiv July 24, 2023.

**Funding:** This work was partially supported by the National Science and Technology Council, the National Center for Theoretical Sciences, and the ST Yau Center in Taiwan.

<sup>†</sup>Department of Mathematics, National Taiwan Normal University, Taipei, Taiwan (lii227857@gmail.com, yue@ntnu.edu.tw).

strated to validate the significantly improved effectiveness of our new algorithm in terms of area-preserving accuracy and computational efficiency.

- (iii) An application to the computation of area-preserving registration mappings between surfaces is demonstrated to show the utility of the new algorithm.

**1.2. Notation.** In this paper, we use the following notation.

- Real-valued vectors are represented using bold letters, such as  $\mathbf{f}$ .
- Real-valued matrices are represented using capital letters, such as  $L$ .
- $I_n$  denotes the identity matrix of size  $n \times n$ .
- Ordered sets of indices are denoted using typewriter letters, such as  $\mathbf{I}$  and  $\mathbf{B}$ .
- The  $i$ th entry of the vector  $\mathbf{f}$  is denoted by  $\mathbf{f}_i$ .
- The subvector of  $\mathbf{f}$ , composed of  $\mathbf{f}_i$  for  $i$  in the set of indices  $\mathbf{I}$ , is represented as  $\mathbf{f}_{\mathbf{I}}$ .
- The  $(i, j)$ th entry of the matrix  $L$  is represented by  $L_{i,j}$ .
- The submatrix of  $L$ , composed of entries  $L_{i,j}$  for  $i$  in the set of indices  $\mathbf{I}$  and  $j$  in the set of indices  $\mathbf{J}$ , is denoted by  $L_{\mathbf{I},\mathbf{J}}$ .
- The set of real numbers is represented by  $\mathbb{R}$ .
- The  $k$ -simplex with vertices  $v_0, \dots, v_k$  is denoted by  $[v_0, \dots, v_k]$ .
- The volume of the  $k$ -simplex  $[v_0, \dots, v_k]$  is represented by  $|[v_0, \dots, v_k]|$ .
- The zero and one vectors or matrices of appropriate sizes are denoted by  $\mathbf{0}$  and  $\mathbf{1}$ , respectively.
- The identity map is denoted as  $\text{id}$ .

**1.3. Organization of the paper.** The remaining part of this paper is organized as follows: In section 2, we introduce the simplicial surfaces, mappings, and the stretch energy functional. Then, we propose the nonlinear CG method of the SEM for computing area-preserving parameterizations of surfaces in section 3. The convergence analysis of the proposed iterative method is provided in section 4. Numerical experiments and a comparison to another state-of-the-art algorithm are demonstrated in section 5. An application of the SEM algorithm to the computation of area-preserving registration mappings is presented in section 6. Concluding remarks are provided in section 7.

**2. Stretch energy of simplicial mappings.** A simplicial surface  $\mathcal{S} \subset \mathbb{R}^3$  is the underlying space of a simplicial 2-complex consisted of  $n$  vertices

$$\mathcal{V}(\mathcal{S}) = \{v_\ell = (v_\ell^1, v_\ell^2, v_\ell^3) \in \mathbb{R}^3\}_{\ell=1}^n,$$

and  $m$  oriented triangular faces

$$\mathcal{F}(\mathcal{S}) = \{\tau_s = [v_{i_s}, v_{j_s}, v_{k_s}] \subset \mathbb{R}^3 \mid v_{i_s}, v_{j_s}, v_{k_s} \in \mathcal{V}(\mathcal{S})\}_{s=1}^m,$$

where the bracket  $[v_{i_s}, v_{j_s}, v_{k_s}]$  denotes a 2-simplex, i.e., a triangle with vertices being  $v_{i_s}, v_{j_s}, v_{k_s}$ . The set of edges is denoted as

$$\mathcal{E}(\mathcal{S}) = \{[v_i, v_j] \subset \mathbb{R}^3 \mid [v_i, v_j, v_k] \in \mathcal{F}(\mathcal{S}) \text{ for some } v_k \in \mathcal{V}(\mathcal{S})\}.$$

A simplicial mapping  $f : \mathcal{S} \rightarrow \mathbb{R}^2$  on  $\mathcal{S}$  is a mapping such that  $f(\mathcal{S})$  is the underlying space of the simplicial 2-complex composed of vertices  $\mathcal{V}(f(\mathcal{S})) = \{f(v_\ell) \in \mathbb{R}^2 \mid v_\ell \in \mathcal{V}(\mathcal{S})\}_{\ell=1}^n$ , edges  $\mathcal{E}(f(\mathcal{S})) = \{[f(v_i), f(v_j)] \subset \mathbb{R}^2 \mid [v_i, v_j] \in \mathcal{E}(\mathcal{S})\}$ , and triangular faces  $\mathcal{F}(f(\mathcal{S})) = \{[f(v_i), f(v_j), f(v_k)] \subset \mathbb{R}^2 \mid [v_i, v_j, v_k] \in \mathcal{F}(\mathcal{S})\}$ . In other words,  $f$  is a piecewise affine mapping that satisfies

$$f|_{\tau_s}(v) = \frac{1}{|\tau_s|} \left( |[v, v_{j_s}, v_{k_s}]| f(v_{i_s}) + |[v_{i_s}, v, v_{k_s}]| f(v_{j_s}) + |[v_{i_s}, v_{j_s}, v]| f(v_{k_s}) \right),$$

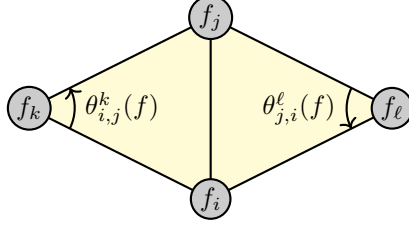


FIG. 1. An illustration of the cotangent weight defined on the image of  $f$ . Here,  $f_i$ ,  $f_j$ ,  $f_k$  and  $f_\ell$  denote  $f(v_i)$ ,  $f(v_j)$ ,  $f(v_k)$  and  $f(v_\ell)$ , respectively.

for every  $\tau_s \in \mathcal{F}(\mathcal{S})$ , where  $|\tau_s|$  denote the area of the triangle  $\tau_s$ . The coefficients

$$(\lambda_i(\tau_s, v), \lambda_j(\tau_s, v), \lambda_k(\tau_s, v)) = \left( \frac{|[v, v_{j_s}, v_{k_s}]|}{|\tau_s|}, \frac{|[v_{i_s}, v, v_{k_s}]|}{|\tau_s|}, \frac{|[v_{i_s}, v_{j_s}, v]|}{|\tau_s|} \right)$$

are called the barycentric coordinates. As a result, the simplicial mapping  $f$  can be represented as a vector

$$\mathbf{f} = (f_1^1, \dots, f_n^1, f_1^2, \dots, f_n^2)^\top \in \mathbb{R}^{2n}.$$

The stretch energy for the simplicial mapping  $f$  is defined as

$$(2.1a) \quad E_S(f) = \frac{1}{2} \mathbf{f}^\top (I_2 \otimes L_S(f)) \mathbf{f},$$

with  $L_S(f)$  being the weighted Laplacian matrix given by

$$(2.1b) \quad [L_S(f)]_{i,j} = \begin{cases} -\sum_{[v_i, v_j, v_k] \in \mathcal{F}(\mathcal{S})} [\omega_S(f)]_{i,j,k} & \text{if } [v_i, v_j] \in \mathcal{E}(\mathcal{S}), \\ -\sum_{\ell \neq i} [L_S(f)]_{i,\ell} & \text{if } j = i, \\ 0 & \text{otherwise,} \end{cases}$$

where  $\omega_S$  is the modified cotangent weight defined as

$$(2.1c) \quad [\omega_S(f)]_{i,j,k} = \frac{\cot(\theta_{i,j}^k(f)) |f([v_i, v_j, v_k])|}{2|[v_i, v_j, v_k]|}$$

in which  $\theta_{i,j}^k(f)$  is the angle opposite to the edge  $[f(v_i), f(v_j)]$  at the point  $f(v_k)$  on the image  $f(\mathcal{S})$ , as illustrated in Figure 1.

The gradient of  $E_S$  in (2.1) can be explicitly formulated as

$$(2.2) \quad \nabla E_S(f) = 2(I_2 \otimes L_S(f)) \mathbf{f}.$$

A detailed derivation can be found in [21]. In particular, suppose  $\mathcal{S}$  is a simply connected open simplicial surface with a boundary  $\partial\mathcal{S}$ . We denote the index sets of entries of  $\mathbf{f}$  correspond to boundary and interior vertices as

$$(2.3) \quad \mathbf{B} = \{b, n+b \mid v_b \in \partial\mathcal{S}\} \quad \text{and} \quad \mathbf{I} = \{1, \dots, 2n\} \setminus \mathbf{B},$$

respectively. Under a given boundary constraint  $\mathbf{f}_\mathbf{B}$ , the gradient of  $E_S$  with respect to the interior vertices can be formulated as

$$(2.4) \quad \nabla_{\mathbf{f}_\mathbf{I}} E_S(f) = 2[I_2 \otimes L_S(f)]_{\mathbf{I},\mathbf{I}} \mathbf{f}_\mathbf{I} + 2[I_2 \otimes L_S(f)]_{\mathbf{I},\mathbf{B}} \mathbf{f}_\mathbf{B}.$$

It is proved that the lower bound of  $E_S(f)$  is the image area  $\mathcal{A}(f)$ , and the equality holds if and only if  $f$  preserves the area [21]. To find a minimizer of  $E_S$ , the fixed-point iteration was adopted in [25], which is formulated as

$$(2.5) \quad [I_2 \otimes L_S(f^{(k)})]_{\mathbf{I}, \mathbf{I}} \mathbf{f}_{\mathbf{I}}^{(k+1)} = -[I_2 \otimes L_S(f^{(k)})]_{\mathbf{I}, \mathbf{B}} \mathbf{b},$$

where  $L_S(f^{(0)}) = L_S(\text{id})$  and  $\mathbf{b}$  is a prescribed boundary map.

**3. Nonlinear CG Methods.** The concept of the nonlinear CG method for solving nonlinear optimization problems was first introduced by Fletcher and Reeves [7]. Given the availability of the explicit formula (2.2) for the objective nonlinear functional (2.1), this concept aligns well with our intended objective.

Suppose an initial map  $\mathbf{f}^{(0)}$  is computed by the fixed-point iteration (2.5) of SEM with  $N$  iteration steps. From (2.4), under the boundary constraint  $\mathbf{f}_{\mathbf{B}}^{(k)} = \mathbf{b}$ , the gradient of  $E_S$  at  $\mathbf{f}^{(0)}$  is formulated as

$$\mathbf{g}^{(0)} = \nabla_{\mathbf{f}_{\mathbf{I}}} E_S(f^{(0)}) = 2[I_2 \otimes L_S(f^{(0)})]_{\mathbf{I}, \mathbf{I}} \mathbf{f}_{\mathbf{I}}^{(0)} + 2[I_2 \otimes L_S(f^{(0)})]_{\mathbf{I}, \mathbf{B}} \mathbf{b}.$$

Then, the interior map is updated along with the negative gradient direction as

$$\mathbf{f}_{\mathbf{I}}^{(1)} = \mathbf{f}_{\mathbf{I}}^{(0)} + \alpha_0 \mathbf{p}^{(0)},$$

where

$$(3.1a) \quad \mathbf{p}^{(0)} = -\mathbf{g}^{(0)},$$

and  $\alpha_0$  is a suitable step size. The choice of step sizes will be discussed in subsection 3.1. Next, suppose we have the descent direction  $\mathbf{p}^{(k)}$ . The conjugate gradient of  $E_S$  at  $\mathbf{f}^{(k+1)}$  is formulated as

$$(3.1b) \quad \mathbf{p}^{(k+1)} = -\mathbf{g}^{(k+1)} + \beta_{k+1} \mathbf{p}^{(k)},$$

where

$$\beta_{k+1} = \frac{\mathbf{g}^{(k+1)\top} \mathbf{g}^{(k+1)}}{\mathbf{g}^{(k)\top} \mathbf{g}^{(k)}}.$$

The map is then updated along with the conjugate gradient direction as

$$\mathbf{f}_{\mathbf{I}}^{(k+1)} = \mathbf{f}_{\mathbf{I}}^{(k)} + \alpha_k \mathbf{p}^{(k)},$$

where

$$\mathbf{p}^{(k+1)} = -\mathbf{g}^{(k+1)} + \beta_{k+1} \mathbf{p}^{(k)}$$

with

$$\mathbf{g}^{(k)} = \nabla_{\mathbf{f}_{\mathbf{I}}} E_S(f^{(k)}) = 2[I_2 \otimes L_S(f^{(k)})]_{\mathbf{I}, \mathbf{I}} \mathbf{f}_{\mathbf{I}}^{(k)} + 2[I_2 \otimes L_S(f^{(k)})]_{\mathbf{I}, \mathbf{B}} \mathbf{f}_{\mathbf{B}}^{(0)}.$$

**3.1. Quadratic approximation of step sizes.** Under the boundary constraint  $\mathbf{f}_{\mathbf{B}} = \mathbf{f}_{\mathbf{B}}^{(0)}$ , the stretch energy can be written as a function of  $\mathbf{f}_{\mathbf{I}}$ . To estimate the optimal step size  $\alpha_k$ , we write  $\Phi^{(k)}(\alpha) = E_S(\mathbf{f}_{\mathbf{I}}^{(k)} + \alpha \mathbf{p}^{(k)})$ . Then,

$$\begin{aligned} \frac{d}{d\alpha} \Phi^{(k)}(\alpha) &= \mathbf{p}^{(k)\top} \nabla_{\mathbf{f}_{\mathbf{I}}} E_S(\mathbf{f}_{\mathbf{I}}^{(k)} + \alpha \mathbf{p}^{(k)}) \\ &= 2\mathbf{p}^{(k)\top} \left( [I_2 \otimes L_S(\mathbf{f}_{\mathbf{I}}^{(k)} + \alpha \mathbf{p}^{(k)})]_{\mathbf{I}, \mathbf{I}} (\mathbf{f}_{\mathbf{I}}^{(k)} + \alpha \mathbf{p}^{(k)}) \right. \\ &\quad \left. + [I_2 \otimes L_S(\mathbf{f}_{\mathbf{I}}^{(k)} + \alpha \mathbf{p}^{(k)})]_{\mathbf{I}, \mathbf{B}} \mathbf{f}_{\mathbf{B}}^{(0)} \right). \end{aligned}$$



The critical point of the function  $\Phi^{(k)}(\alpha)$  satisfies  $\frac{d}{d\alpha}\Phi^{(k)}(\alpha) = 0$ . However, deriving an explicit formulation for  $\frac{d}{d\alpha}\Phi^{(k)}(\alpha)$  poses a challenge due to the dependence of the matrix  $[I_2 \otimes L_S(\mathbf{f}_I^{(k)} + \alpha\mathbf{p}^{(k)})]_{I,I}$  on  $\alpha$  as well. To remedy this drawback, we approximate the function  $\Phi^{(k)}$  by a quadratic function

$$(3.2) \quad \tilde{\Phi}^{(k)}(\alpha) = a_2^{(k)}\alpha^2 + a_1^{(k)}\alpha + a_0^{(k)}$$

that satisfies

$$\begin{cases} \tilde{\Phi}^{(k)}(0) = \Phi^{(k)}(0) = E_S(f^{(k)}), \\ \frac{d}{d\alpha}\tilde{\Phi}^{(k)}(0) = \frac{d}{d\alpha}\Phi^{(k)}(0) = 2\mathbf{p}^{(k)\top} ([I_2 \otimes L_S(\mathbf{f}_I^{(k)})]_{I,I}\mathbf{f}_I^{(k)} + [I_2 \otimes L_S(\mathbf{f}_I^{(k)})]_{I,B}\mathbf{f}_B^{(0)}), \\ \tilde{\Phi}^{(k)}(\alpha_{k-1}) = \Phi^{(k)}(\alpha_{k-1}) = E_S(\mathbf{f}_I^{(k)} + \alpha_{k-1}\mathbf{p}^{(k)}). \end{cases}$$

The coefficients in (3.2) can be explicitly formulated as

$$\begin{aligned} a_0^{(k)} &= \Phi^{(k)}(0), \quad a_1^{(k)} = \frac{d}{d\alpha}\Phi^{(k)}(0), \quad \text{and} \\ a_2^{(k)} &= \frac{1}{\alpha_{k-1}^2} \left( \Phi^{(k)}(\alpha_{k-1}) - \Phi^{(k)}(0) - \alpha_{k-1} \frac{d}{d\alpha}\Phi^{(k)}(0) \right). \end{aligned}$$

The step size  $\alpha_k$  is then chosen to satisfy  $\frac{d}{d\alpha}\tilde{\Phi}(\alpha_k) = 0$ , which implies

$$(3.3) \quad \alpha_k = \frac{-\frac{d}{d\alpha}\Phi^{(k)}(0)}{2a_2^{(k)}} = \frac{-\alpha_{k-1}^2 \frac{d}{d\alpha}\Phi^{(k)}(0)}{2(\Phi^{(k)}(\alpha_{k-1}) - \Phi^{(k)}(0) - \alpha_{k-1} \frac{d}{d\alpha}\Phi^{(k)}(0))}.$$

**3.2. Preconditioner.** To accelerate the convergence of the CG method, we incorporate a preconditioner  $M = [I_2 \otimes L_S(f^{(0)})]_{I,I}$ , which serves as an approximation of  $[I_2 \otimes L_S(f^{(k)})]_{I,I}$  for  $k \in \mathbb{N}$ . Then, the conjugate gradient direction (3.1) is replaced with

$$(3.4a) \quad \mathbf{p}^{(0)} = -M^{-1}\mathbf{g}^{(0)}$$

and

$$(3.4b) \quad \mathbf{p}^{(k+1)} = -M^{-1}\mathbf{g}^{(k+1)} + \beta_{k+1}\mathbf{p}^{(k)},$$

where

$$\beta_{k+1} = \frac{\mathbf{g}^{(k+1)\top} M^{-1}\mathbf{g}^{(k+1)}}{\mathbf{g}^{(k)\top} M^{-1}\mathbf{g}^{(k)}}.$$

In practice, we compute the preordered Cholesky decomposition

$$(3.5) \quad R^\top R = P^\top M P,$$

where  $R$  is an upper triangular matrix and  $P$  is the approximate minimum degree permutation matrix [4]. Then, linear systems of the form  $M\mathbf{x} = \mathbf{r}$  can be efficiently solved by solving lower and upper triangular systems

$$(3.6a) \quad R^\top \mathbf{y} = P^\top \mathbf{r} \quad \text{and} \quad R\mathbf{z} = \mathbf{y}.$$

Ultimately, the solution to the system is given by

$$(3.6b) \quad \mathbf{x} = P\mathbf{z}.$$

The detailed computational procedure is summarized in Algorithm 3.1.

---

**Algorithm 3.1** Nonlinear CG method of SEM for area-preserving maps

---

**Require:** A simply connected open mesh  $\mathcal{S}$  and a initial map  $\mathbf{f}$ .

**Ensure:** An area-preserving map  $f : \mathcal{S} \rightarrow \mathbb{D}$ .

- 1: Let  $\mathbf{I}$  and  $\mathbf{B}$  be defined in (2.3).
  - 2: Define the matrix  $L = I_2 \otimes L_S(f)$  as in (2.1b).
  - 3: Let  $M = L_{\mathbf{I}, \mathbf{I}}$ .
  - 4: Compute the preordered Cholesky decomposition  $R^\top R = P^\top M P$ , as in (3.5).
  - 5: Let  $\mathbf{g} = L_{\mathbf{I}, \mathbf{I}} \mathbf{f}_{\mathbf{I}} + L_{\mathbf{I}, \mathbf{B}} \mathbf{f}_{\mathbf{B}}$ .
  - 6: Solve  $M \mathbf{h} = \mathbf{g}$  by (3.6).
  - 7: Let  $\mathbf{p} = -\mathbf{h}$ .
  - 8: Define an initial guess  $\alpha$ .
  - 9: **while** not converge **do**
  - 10:   Update  $\alpha$  as in (3.3).
  - 11:   Update  $\mathbf{f} \leftarrow \mathbf{f} + \alpha \mathbf{p}$ .
  - 12:   Update  $L \leftarrow I_2 \otimes L_S(f)$
  - 13:   Let  $\lambda = \mathbf{h}^\top \mathbf{g}$ .
  - 14:   Update  $\mathbf{g} = L_{\mathbf{I}, \mathbf{I}} \mathbf{f}_{\mathbf{I}} + L_{\mathbf{I}, \mathbf{B}} \mathbf{f}_{\mathbf{B}}$ .
  - 15:   Solve  $M \mathbf{h} = \mathbf{g}$  by (3.6).
  - 16:   Update  $\beta = (\mathbf{h}^\top \mathbf{g}) / \lambda$ .
  - 17:   Update  $\mathbf{p} \leftarrow -\mathbf{h} + \beta \mathbf{p}$ .
  - 18: **end while**
- 

**4. Convergence analysis.** In this section, we prove the global convergence of the preconditioned CG method of the SEM Algorithm 3.1. It is important to note that the boundary map is subject to the constraint of being constant, denoted as  $\mathbf{f}_{\mathbf{B}} = \mathbf{f}_{\mathbf{B}}^{(0)}$ . For the sake of simplicity, we use the notation  $\nabla E_S(f^{(k)}) \equiv \nabla_{\mathbf{f}_{\mathbf{I}}} E_S(f^{(k)})$ , as defined in (2.4).

First, we introduce the strong Wolfe conditions, denoted as (4.1), which play a vital role in proving the convergence of Algorithm 3.1. These conditions are expressed as follows:

$$(4.1a) \quad E_S(\mathbf{f}_{\mathbf{I}}^{(k)} + \alpha_k \mathbf{p}^{(k)}) \leq E_S(f^{(k)}) + c_1 \alpha_k \nabla E_S(f^{(k)})^\top \mathbf{p}^{(k)},$$

$$(4.1b) \quad |\nabla E_S(\mathbf{f}_{\mathbf{I}}^{(k)} + \alpha_k \mathbf{p}^{(k)})^\top \mathbf{p}^{(k)}| \leq c_2 |\nabla E_S(f^{(k)})^\top \mathbf{p}^{(k)}|,$$

with  $0 < c_1 < c_2 < 1$ . Since  $E_S(f) \geq \mathcal{A}(f)$  is bounded below, the existence of such  $\alpha_k$  is guaranteed by applying [14, Lemma 3.1], as stated in the following lemma.

**LEMMA 4.1** ([14, Lemma 3.1]). *Let  $\mathbf{p}^{(k)}$  be a descent direction at  $\mathbf{f}_{\mathbf{I}}^{(k)}$ . Suppose  $0 < c_1 < c_2 < 1$ . Then, there exist intervals of step lengths satisfying the strong Wolfe conditions (4.1).*

Observing that Lemma 4.1 requires the assumption that  $\mathbf{p}^{(k)}$  must be a descent direction at  $\mathbf{f}_{\mathbf{I}}^{(k)}$ . When a preconditioner  $M$  is considered, a vital inequality is required to ensure that  $\mathbf{p}^{(k)}$  is always a descent direction at  $\mathbf{f}_{\mathbf{I}}^{(k)}$ . The inequality is stated in the following lemma, which is a variant of [14, Lemma 5.6].

**LEMMA 4.2.** *Given a preconditioner  $M$  with a symmetric positive definite inverse. Suppose the step size  $\alpha_k$  satisfies the strong Wolfe conditions (4.1). Then, the vector*

$\mathbf{p}^{(k)}$  satisfies

$$(4.2) \quad -\frac{1}{1-c_2} \leq \frac{\nabla E_S(f^{(k)})^\top \mathbf{p}^{(k)}}{\|\nabla E_S(f^{(k)})\|_{M^{-1}}^2} \leq \frac{2c_2-1}{1-c_2},$$

for all  $k \geq 0$ , where  $\|\cdot\|_{M^{-1}}$  denotes the  $M^{-1}$ -norm defined as  $\|\mathbf{v}\|_{M^{-1}} = \sqrt{\mathbf{v}^\top M^{-1} \mathbf{v}}$ .

*Proof.* For  $k = 0$ , from (3.4a), we have

$$\frac{\nabla E_S(f^{(0)})^\top \mathbf{p}^{(0)}}{\|\nabla E_S(f^{(0)})\|_{M^{-1}}^2} = \frac{-\nabla E_S(f^{(0)})^\top M^{-1} \mathbf{g}^{(0)}}{\|\nabla E_S(f^{(0)})\|_{M^{-1}}^2} = \frac{-\|\nabla E_S(f^{(0)})\|_{M^{-1}}^2}{\|\nabla E_S(f^{(0)})\|_{M^{-1}}^2} = -1.$$

Next, we assume (4.2) holds for some  $k = n$ . Then, from (3.4b), we have

$$(4.3) \quad \begin{aligned} \frac{\nabla E_S(f^{(n+1)})^\top \mathbf{p}^{(n+1)}}{\|\nabla E_S(f^{(n+1)})\|_{M^{-1}}^2} &= \frac{\nabla E_S(f^{(n+1)})^\top M^{-1} \mathbf{g}^{(n+1)}}{\|\nabla E_S(f^{(n+1)})\|_{M^{-1}}^2} + \beta_{n+1} \frac{\nabla E_S(f^{(n+1)})^\top \mathbf{p}^{(n)}}{\|\nabla E_S(f^{(n+1)})\|_{M^{-1}}^2} \\ &= -1 + \frac{\mathbf{g}^{(n+1)\top} M^{-1} \mathbf{g}^{(n+1)}}{\mathbf{g}^{(n)\top} M^{-1} \mathbf{g}^{(n)}} \frac{\nabla E_S(f^{(n+1)})^\top \mathbf{p}^{(n)}}{\|\nabla E_S(f^{(n+1)})\|_{M^{-1}}^2} \\ &= -1 + \frac{\nabla E_S(f^{(n+1)})^\top \mathbf{p}^{(n)}}{\|\nabla E_S(f^{(n)})\|_{M^{-1}}^2}. \end{aligned}$$

By (4.1b), we have

$$|\nabla E_S(f^{(n+1)})^\top \mathbf{p}^{(n)}| \leq -c_2 \nabla E_S(f^{(n)})^\top \mathbf{p}^{(n)},$$

i.e.,

$$(4.4) \quad c_2 \nabla E_S(f^{(n)})^\top \mathbf{p}^{(n)} \leq \nabla E_S(f^{(n+1)})^\top \mathbf{p}^{(n)} \leq -c_2 \nabla E_S(f^{(n)})^\top \mathbf{p}^{(n)}.$$

As a result, from (4.3) and (4.4), we have

$$-1 + c_2 \frac{\nabla E_S(f^{(n)})^\top \mathbf{p}^{(n)}}{\|\nabla E_S(f^{(n)})\|_{M^{-1}}^2} \leq \frac{\nabla E_S(f^{(n+1)})^\top \mathbf{p}^{(n+1)}}{\|\nabla E_S(f^{(n+1)})\|_{M^{-1}}^2} \leq -1 - c_2 \frac{\nabla E_S(f^{(n)})^\top \mathbf{p}^{(n)}}{\|\nabla E_S(f^{(n)})\|_{M^{-1}}^2}.$$

Then, from the induction hypothesis, we have

$$-1 - \frac{c_2}{1-c_2} \leq \frac{\nabla E_S(f^{(n+1)})^\top \mathbf{p}^{(n+1)}}{\|\nabla E_S(f^{(n+1)})\|_{M^{-1}}^2} \leq -1 + \frac{c_2}{1-c_2},$$

i.e.,

$$-\frac{1}{1-c_2} \leq \frac{\nabla E_S(f^{(n+1)})^\top \mathbf{p}^{(n+1)}}{\|\nabla E_S(f^{(n+1)})\|_{M^{-1}}^2} \leq \frac{2c_2-1}{1-c_2},$$

which shows (4.2) holds for  $k = n + 1$ .  $\square$

In particular, when  $c_2$  in (4.1b) satisfies  $0 < c_2 < \frac{1}{2}$ , Lemma 4.2 guarantees the vector  $\mathbf{p}^{(k)}$  being a descent direction at  $\mathbf{f}^{(k)}$ , which is stated in the following corollary.

**COROLLARY 4.3.** *Suppose the step size  $\alpha_k$  satisfies the strong Wolfe conditions (4.1) with  $0 < c_2 < \frac{1}{2}$ . Then, the vector  $\mathbf{p}^{(k)}$  is a descent direction at  $\mathbf{f}^{(k)}$ .*

*Proof.* Noting that the function  $\varphi(x) = \frac{2x-1}{1-x}$  is monotonically increasing on  $[0, \frac{1}{2}]$  with  $\varphi(0) = -1$  and  $\varphi(\frac{1}{2}) = 0$ . From the assumption  $0 < c_2 < \frac{1}{2}$  and Lemma 4.2, we have

$$\frac{\nabla E_S(f^{(k)})^\top \mathbf{p}^{(k)}}{\|\nabla E_S(f^{(k)})\|_{M^{-1}}^2} \leq \frac{2c_2 - 1}{1 - c_2} < 0.$$

Hence  $\nabla E_S(f^{(k)})^\top \mathbf{p}^{(k)} < 0$  and, therefore, the vector  $\mathbf{p}^{(k)}$  is a descent direction at  $\mathbf{f}^{(k)}$ .  $\square$

Noting that the stretch energy  $E_S(f) \leq \mathcal{A}(f)$  is bounded below, and that  $E_S$  is continuously differentiable. In addition,  $\nabla E_S$  is Lipschitz continuous. To extend the Lipschitz continuity in  $M$ -norm, we provide the following lemma.

LEMMA 4.4. *Let  $M$  be a symmetric positive definite matrix and  $f : \mathbb{R}^n \rightarrow \mathbb{R}^n$  be Lipschitz continuous with respect to the Euclidean norm, i.e.,*

$$\|f(\mathbf{x}) - f(\mathbf{y})\| \leq c_f \|\mathbf{x} - \mathbf{y}\|,$$

for some constant  $c_f \geq 0$ . Then it also satisfies Lipschitz continuity in the  $M$ -norm induced by  $M$ , i.e.,

$$\|f(\mathbf{x}) - f(\mathbf{y})\|_M \leq m_f \|\mathbf{x} - \mathbf{y}\|_M,$$

for some constant  $m_f \geq 0$ .

*Proof.* Since  $M$  is symmetric positive definite,  $M$  is invertible and there exist symmetric positive definite matrices  $M^{1/2}$  and  $M^{-1/2}$  that satisfies  $M = M^{1/2}M^{1/2}$  and  $M^{-1} = M^{-1/2}M^{-1/2}$ . It follows that

$$\|\mathbf{x}\|_M^2 = \mathbf{x}^\top M \mathbf{x} = (M^{1/2} \mathbf{x})^\top M^{1/2} \mathbf{x} = \|M^{1/2} \mathbf{x}\|^2,$$

and

$$(4.5) \quad \|\mathbf{x}\|^2 = \mathbf{x}^\top \mathbf{x} = (M^{-1/2} \mathbf{x})^\top M M^{-1/2} \mathbf{x} = \|M^{-1/2} \mathbf{x}\|_M^2.$$

Therefore,

$$\begin{aligned} \|f(\mathbf{x}) - f(\mathbf{y})\|_M &= \|M^{1/2}(f(\mathbf{x}) - f(\mathbf{y}))\| \leq \|M^{1/2}\| \|f(\mathbf{x}) - f(\mathbf{y})\| \\ &\leq c_f \|M^{1/2}\| \|\mathbf{x} - \mathbf{y}\| \leq c_f \|M^{1/2}\| \|M^{-1/2}\|_M \|\mathbf{x} - \mathbf{y}\|_M. \end{aligned}$$

The constant  $m_f = c_f \|M^{1/2}\| \|M^{-1/2}\|_M \geq 0$ .  $\square$

Under the assumption that  $\alpha_k$  satisfies the Wolfe conditions (4.1) with  $0 < c_2 < \frac{1}{2}$  the modified Zoutendijk's condition would also hold, which is stated as follows.

LEMMA 4.5 (modified Zoutendijk's condition). *Suppose  $\nabla E_S$  is Lipschitz continuous, and the step size  $\alpha_k$  satisfies the strong Wolfe conditions (4.1) with  $0 < c_2 < \frac{1}{2}$ . Then, the vector  $\mathbf{p}^{(k)}$  satisfies*

$$(4.6) \quad \sum_{k=0}^{\infty} \cos^2 \theta_M^{(k)} \|\nabla E_S(f^{(k)})\|_{M^{-1}}^2 < \infty,$$

where  $\theta_M^{(k)}$  is defined as

$$(4.7) \quad \cos \theta_M^{(k)} = -\frac{\nabla E_S(f^{(k)})^\top \mathbf{p}^{(k)}}{\|\nabla E_S(f^{(k)})\|_{M^{-1}} \|\mathbf{p}^{(k)}\|_{M^{-1}}},$$

where  $M^{-1}$  is a symmetric positive definite matrix.

*Proof.* Since the step size  $\alpha_k$  satisfies Equation (4.1), by Corollary 4.3,  $\mathbf{p}^{(k)}$  is a descent direction at  $\mathbf{f}_\Gamma^{(k)}$  so that (4.1b) can be written as

$$(4.8) \quad \nabla E_S(f^{(k+1)})^\top \mathbf{p}^{(k)} \geq c_2 \nabla E_S(f^{(k)})^\top \mathbf{p}^{(k)}.$$

By subtracting  $\nabla E_S(f^{(k)})^\top \mathbf{p}^{(k)}$  in both sides of (4.8), we obtain

$$(\nabla E_S(f^{(k+1)}) - \nabla E_S(f^{(k)}))^\top \mathbf{p}^{(k)} \geq (c_2 - 1) \nabla E_S(f^{(k)})^\top \mathbf{p}^{(k)}.$$

By applying Lemma 4.4 and (4.5), we have

$$\begin{aligned} (c_2 - 1) \nabla E_S(f^{(k)})^\top \mathbf{p}^{(k)} &\leq (\nabla E_S(f^{(k+1)}) - \nabla E_S(f^{(k)}))^\top \mathbf{p}^{(k)} \\ &\leq \|\nabla E_S(f^{(k+1)}) - \nabla E_S(f^{(k)})\| \|\mathbf{p}^{(k)}\| \\ &\leq c_E \|\mathbf{f}_\Gamma^{(k+1)} - \mathbf{f}_\Gamma^{(k)}\| \|\mathbf{p}^{(k)}\| \\ &= c_E \|M^{1/2} \mathbf{f}_\Gamma^{(k+1)} - \mathbf{f}_\Gamma^{(k)}\|_{M^{-1}} \|M^{1/2} \mathbf{p}^{(k)}\|_{M^{-1}} \\ &\leq c_E \|M^{1/2}\|_{M^{-1}}^2 \|\mathbf{f}_\Gamma^{(k+1)} - \mathbf{f}_\Gamma^{(k)}\|_{M^{-1}} \|\mathbf{p}^{(k)}\|_{M^{-1}} \\ &= c_E \|M^{1/2}\|_{M^{-1}}^2 \alpha_k \|\mathbf{p}^{(k)}\|_{M^{-1}}^2. \end{aligned}$$

As a result,

$$\alpha_k \geq \frac{c_2 - 1}{c_E \|M^{1/2}\|_{M^{-1}}^2} \frac{\nabla E_S(f^{(k)})^\top \mathbf{p}^{(k)}}{\|\mathbf{p}^{(k)}\|_{M^{-1}}^2}.$$

By substituting  $\alpha_k$  into (4.1a), we obtain

$$(4.9) \quad E_S(f^{(k+1)}) \leq E_S(f^{(k)}) - \frac{c (\nabla E_S(f^{(k)})^\top \mathbf{p}^{(k)})^2}{\|\mathbf{p}^{(k)}\|_{M^{-1}}^2}$$

$$(4.10) \quad = E_S(f^{(k)}) - c \cos^2 \theta_M^{(k)} \|E_S(f^{(k)})\|_{M^{-1}}^2,$$

where  $c = \frac{c_1(1-c_2)}{c_E \|M^{1/2}\|_{M^{-1}}^2}$  and  $\cos \theta_M^{(k)}$  is defined as (4.7). The recursive inequality (4.10) implies

$$E_S(f^{(k+1)}) \leq E_S(f^{(0)}) - c \sum_{j=0}^k \cos^2 \theta_M^{(j)} \|E_S(f^{(j)})\|_{M^{-1}}^2.$$

In other words,

$$(4.11) \quad \sum_{j=0}^k \cos^2 \theta_M^{(j)} \|\nabla E_S(f^{(j)})\|_{M^{-1}}^2 = \frac{1}{c} (E_S(f^{(0)}) - E_S(f^{(k+1)})).$$

Noting that  $E_S(f)$  is bounded below, which implies  $E_S(f^{(0)}) - E_S(f^{(k+1)})$  is bounded above. Therefore, by taking the limit of (4.11), we obtain (4.6) as desired.  $\square$

Lemma 4.5 implies that as  $\cos^2 \theta_k \|\nabla E_S(f^{(k)})\|_{M^{-1}}^2$  tends to zero, the gradient descent method converges because  $\theta_k = 0$  and  $\cos \theta_k = 1$ . In the case of the nonlinear preconditioned CG method, where  $\mathbf{p}^{(k)}$  is a descent direction with  $\theta_k < \frac{\pi}{2}$ , we have  $\cos \theta_k > 0$  for all  $k$ . However, it is still possible for  $\cos \theta_k$  to approach zero, which means that  $\|\nabla E_S(f^{(k)})\|_{M^{-1}}$  may not converge to zero. Fortunately, we can apply Lemmas 4.2 and 4.5 to establish a global convergence theorem for the nonlinear preconditioned CG method, which is stated as follows.

THEOREM 4.6. *Suppose  $\nabla E_S$  is Lipschitz continuous, and the step size  $\alpha_k$  satisfies the strong Wolfe conditions (4.1) with  $0 < c_1 < c_2 < \frac{1}{2}$ . Then,*

$$(4.12) \quad \liminf_{k \rightarrow \infty} \|\nabla E_S(f^{(k)})\|_{M^{-1}} = 0,$$

where  $M^{-1}$  is a symmetric positive definite matrix.

*Proof.* We prove (4.12) by contradiction. Assume on the contrary that

$$\liminf_{k \rightarrow \infty} \|\nabla E_S(f^{(k)})\|_{M^{-1}} \neq 0,$$

i.e., there exist  $N \in \mathbb{N}$  and  $\gamma > 0$  such that

$$(4.13) \quad \|\nabla E_S(f^{(k)})\|_{M^{-1}} \geq \gamma,$$

for every  $k > N$ . Let  $\theta_k$  be defined as (4.7). Then, by Lemma 4.2 together with (4.7), we have

$$-\frac{1}{1-c_2} \leq -\cos \theta_k \frac{\|\mathbf{p}^{(k)}\|_{M^{-1}}}{\|\nabla E_S(f^{(k)})\|_{M^{-1}}} \leq \frac{2c_2-1}{1-c_2}.$$

Equivalently,

$$(4.14) \quad \frac{1-2c_2}{1-c_2} \frac{\|\nabla E_S(f^{(k)})\|_{M^{-1}}}{\|\mathbf{p}^{(k)}\|_{M^{-1}}} \leq \cos \theta_k \leq \frac{1}{1-c_2} \frac{\|\nabla E_S(f^{(k)})\|_{M^{-1}}}{\|\mathbf{p}^{(k)}\|_{M^{-1}}}.$$

By Lemma 4.5, we have

$$(4.15) \quad \sum_{k=0}^{\infty} \cos^2 \theta_k \|\nabla E_S(f^{(k)})\|_{M^{-1}}^2 < \infty.$$

Hence, with (4.14) and (4.15), we obtain

$$(4.16) \quad \sum_{k=0}^{\infty} \frac{\|\nabla E_S(f^{(k)})\|_{M^{-1}}^4}{\|\mathbf{p}^{(k)}\|_{M^{-1}}^2} < \infty.$$

By Lemma 4.2, we have

$$-\nabla E_S(f^{(k)})^\top \mathbf{p}^{(k)} \leq \frac{1}{1-c_2} \|\nabla E_S(f^{(k)})\|_{M^{-1}}^2.$$

Then, by (4.1b), we obtain

$$(4.17) \quad |\nabla E_S(f^{(k)})^\top \mathbf{p}^{(k-1)}| \leq -c_2 \nabla E_S(f^{(k-1)})^\top \mathbf{p}^{(k-1)} \leq \frac{c_2}{1-c_2} \|\nabla E_S(f^{(k-1)})\|_{M^{-1}}^2.$$

Hence, by (4.17), we have

$$(4.18) \quad \begin{aligned} \|\mathbf{p}^{(k)}\|_M^2 &= \|-M^{-1}\nabla E_S(f^{(k)}) + \beta_k \mathbf{p}^{(k-1)}\|_M^2 \\ &= \|M^{-1}\nabla E_S(f^{(k)})\|_M^2 - 2\beta_k (M^{-1}\nabla E_S(f^{(k)}))^\top (M\mathbf{p}^{(k-1)}) + \beta_k^2 \|\mathbf{p}^{(k-1)}\|_M^2 \\ &\leq \|\nabla E_S(f^{(k)})\|_{M^{-1}}^2 + 2\beta_k |\nabla E_S(f^{(k)})^\top \mathbf{p}^{(k-1)}| + \beta_k^2 \|\mathbf{p}^{(k-1)}\|_M^2 \\ &\leq \|\nabla E_S(f^{(k)})\|_{M^{-1}}^2 + \frac{2c_2}{1-c_2} \beta_k \|\nabla E_S(f^{(k-1)})\|_{M^{-1}}^2 + \beta_k^2 \|\mathbf{p}^{(k-1)}\|_M^2 \\ &= \|\nabla E_S(f^{(k)})\|_{M^{-1}}^2 + \frac{2c_2}{1-c_2} \|\nabla E_S(f^{(k)})\|_{M^{-1}}^2 + \beta_k^2 \|\mathbf{p}^{(k-1)}\|_M^2 \\ &= \left(\frac{1+c_2}{1-c_2}\right) \|\nabla E_S(f^{(k)})\|_{M^{-1}}^2 + \beta_k^2 \|\mathbf{p}^{(k-1)}\|_M^2. \end{aligned}$$

Let  $c_3 = (1 + c_2)/(1 - c_2)$ . The recursive inequality (4.18) with  $\mathbf{p}^{(0)} = M^{-1}\nabla E_S(f^{(0)})$  implies

$$(4.19) \quad \|\mathbf{p}^{(k)}\|_M^2 \leq c_3 \sum_{i=0}^k \left( \prod_{j=i+1}^k \beta_j^2 \right) \|\nabla E_S(f^{(i)})\|_{M^{-1}}^2.$$

Recall that  $\beta_k = \|\nabla E_S(f^{(k)})\|_{M^{-1}}^2 / \|\nabla E_S(f^{(k-1)})\|_{M^{-1}}^2$ , the product

$$(4.20) \quad \prod_{j=i+1}^k \beta_j^2 = \frac{\|\nabla E_S(f^{(k)})\|_{M^{-1}}^4}{\|\nabla E_S(f^{(i)})\|_{M^{-1}}^4}.$$

By substituting (4.20) into (4.19), we obtain

$$(4.21) \quad \|\mathbf{p}^{(k)}\|_M^2 \leq c_3 \|\nabla E_S(f^{(k)})\|_{M^{-1}}^4 \sum_{i=0}^k \frac{1}{\|\nabla E_S(f^{(i)})\|_{M^{-1}}^2}.$$

In addition, by (4.13) and the inequality  $\|\nabla E_S(f^{(k)})\|_{M^{-1}}^2 \leq \|\nabla E_S(f^{(j)})\|_{M^{-1}}^2$  for  $j \leq k$ , we have, for  $k > N$ ,

$$(4.22) \quad \sum_{i=0}^k \frac{1}{\|\nabla E_S(f^{(i)})\|_{M^{-1}}^2} \leq \sum_{i=0}^k \frac{1}{\|\nabla E_S(f^{(k)})\|_{M^{-1}}^2} \leq \frac{k}{\gamma^2}.$$

Since  $\nabla E_S$  is Lipschitz continuous, there exists  $\bar{\gamma}$  such that  $\|\nabla E_S(f^{(k)})\|_{M^{-1}} \leq \bar{\gamma}$  for all  $k$ . As a result, from (4.21) and (4.22), for  $k > N$ ,

$$\|\mathbf{p}^{(k)}\|_M^2 \leq \frac{c_3 \bar{\gamma}^4}{\gamma^2} k.$$

This implies that

$$(4.23) \quad \sum_{k=1}^{\infty} \frac{1}{\|\mathbf{p}^{(k)}\|_M^2} \geq \omega \sum_{k=1}^{\infty} \frac{1}{k},$$

for some  $\omega > 0$ . On the other hand, from (4.13) and (4.16), we have

$$\sum_{k=0}^{\infty} \frac{1}{\|\mathbf{p}^{(k)}\|_M^2} < \infty,$$

which contradicts to (4.23). □

**5. Numerical experiments.** We present the numerical results of the disk area-preserving parameterizations computed by the preconditioned CG method for SEM, Algorithm 3.1. The experiments were performed using MATLAB on a MacBook Pro M1 with 16 GB RAM. The benchmark triangular mesh models, shown in Figure 2, were acquired from reputable sources such as the AIM@SHAPE shape repository [1], the Stanford 3D scanning repository [2], and Sketchfab [3]. To ensure consistency, certain mesh models underwent resampling or modification to guarantee that each triangular face contains at least one interior vertex.

In Figure 3, we present images of area-preserving parameterizations computed by the proposed nonlinear CG method (Algorithm 3.1). It is important to emphasize that

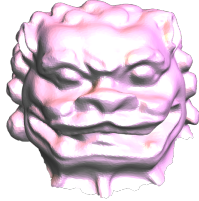







Model Name	Chinese Lion	Femur	Max Planck	Left Hand
# Faces	34,421	43,301	82,977	105,780
# Vertices	17,334	21,699	41,588	53,011
				
Model Name	Knit Cap Man	Bimba Statue	Buddha	Nefertiti Statue
# Faces	118,849	433,040	945,722	1,992,801
# Vertices	59,561	216,873	473,362	996,838
				

FIG. 2. The benchmark triangular mesh models used in this paper.

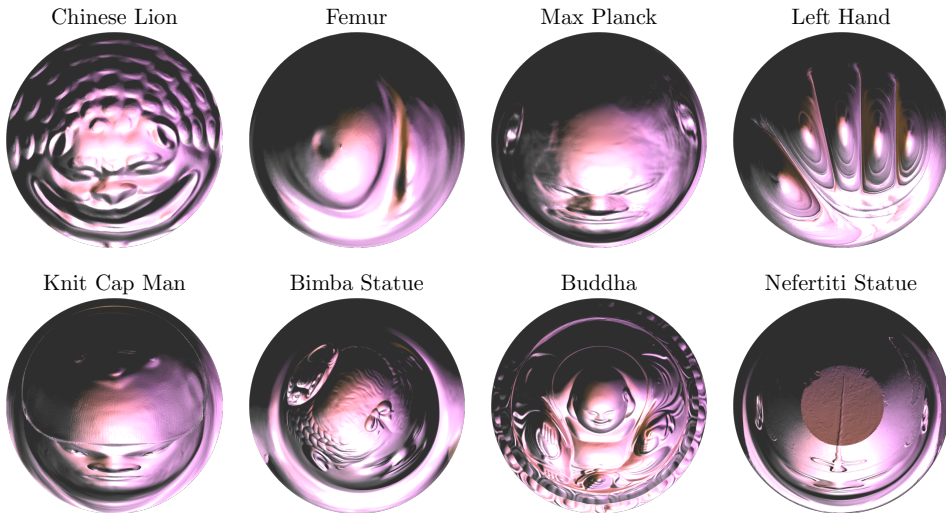


FIG. 3. The area-preserving parameterizations of benchmark triangular mesh models computed by Algorithm 3.1 with the boundary mapping being the disk-shaped arc-length parameterization.

all parameterizations displayed in the figure are bijective, meaning no folded triangles occur in the resulting mappings. Consequently, each mapping can be utilized as a reliable surface parameterization for subsequent applications.

To quantify the local area distortion, we compute the mean and standard devia-



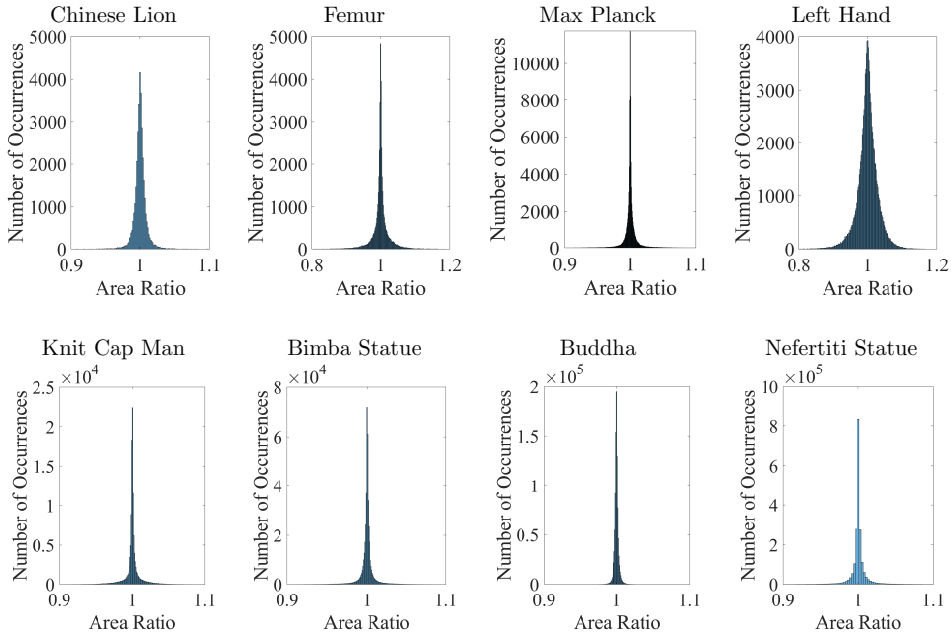


FIG. 4. Histograms of the area ratios  $R_A(f, \tau)$ , representing the local area distortions, for the area-preserving parameterizations of benchmark mesh models computed using the proposed nonlinear CG method (Algorithm 3.1).

tion (SD) of the local area ratio, denoted as  $R_A(f, \tau)$ , defined as

$$(5.1) \quad R_A(f, \tau) = \frac{|f(\tau)|}{|\tau|},$$

where  $f$  is the computed area-preserving parameterization and  $\tau$  represents a triangular face in the set  $\mathcal{F}(\mathcal{S})$ . Evaluating the mean and SD involves considering all triangular faces in  $\mathcal{F}(\mathcal{S})$ . It is evident that an area-preserving mapping  $f$  has the property that

$$\text{mean}_{\tau \in \mathcal{F}(\mathcal{S})} R_A(f, \tau) = 1 \quad \text{and} \quad \text{SD}_{\tau \in \mathcal{F}(\mathcal{S})} R_A(f, \tau) = 0.$$

Figure 4 illustrates histograms of the distribution of area ratios  $R_A(f, \tau)$ , defined in (5.1), for the area-preserving parameterizations of benchmark mesh models computed by Algorithm 3.1. The histograms reveal a concentrated distribution of area ratios around 1, with radii measuring less than 0.2. This observation indicates that the resulting mappings are nearly area-preserving.

In Table 1, we provide a comparison between the proposed nonlinear CG method of SEM, Algorithm 3.1, for computing area-preserving parameterizations and a state-of-the-art fixed-point iterative algorithm of SEM [25]. The maximal number of iterations of both algorithms is set to 50. The comparison is based on the criteria of area-preserving accuracy and computational efficiency. The global area distortion is measured by the authalic energy defined as

$$(5.2) \quad E_A(f) = E_S(f) - \mathcal{A}(f),$$

where  $\mathcal{A}(f)$  measures the area of the image of  $f$ . The authalic energy (5.2) has the property that  $E_A(f) \geq 0$ , and the equality holds if and only if  $f$  is area-preserving [21].

TABLE 1

The mean and SD of area ratios, defined in (5.1), the authalic energy  $E_A$  specified in (5.2), and the computational time required for computing the area-preserving parameterization using both the fixed-point method [25] and the nonlinear CG method (Algorithm 3.1). The maximal number of iterations of both algorithms is set to 50. It is important to note that all resulting mappings are bijective, ensuring the absence of folded triangles in the images.

Model name	Fixed-point method [25]				Nonlinear CG method (Algorithm 3.1)			
	Area ratios		$E_A(f)$	Time (secs.)	Area ratios		$E_A(f)$	Time (secs.)
	Mean	SD			Mean	SD		
Chinese Lion	1.00	0.0195	$1.15 \times 10^{-3}$	1.83	1.00	0.0124	$4.29 \times 10^{-4}$	1.43
Femur	1.00	0.0472	$6.83 \times 10^{-3}$	2.64	1.00	0.0282	$2.30 \times 10^{-3}$	1.81
Max Planck	1.00	0.0178	$9.88 \times 10^{-4}$	5.23	1.00	0.0113	$3.97 \times 10^{-4}$	3.05
Left Hand	1.00	0.0493	$7.68 \times 10^{-3}$	6.46	1.00	0.0309	$2.88 \times 10^{-3}$	3.85
Knit Cap Man	1.00	0.0190	$1.14 \times 10^{-3}$	7.63	1.00	0.0116	$4.00 \times 10^{-4}$	4.52
Bimba Statue	1.00	0.0164	$8.21 \times 10^{-4}$	35.45	1.00	0.0103	$3.05 \times 10^{-4}$	20.81
Buddha	1.00	0.0045	$6.00 \times 10^{-5}$	102.29	1.00	0.0033	$3.17 \times 10^{-5}$	30.48
Nefertiti Statue	1.00	0.0244	$4.08 \times 10^{-3}$	175.20	1.00	0.0171	$1.62 \times 10^{-3}$	99.39

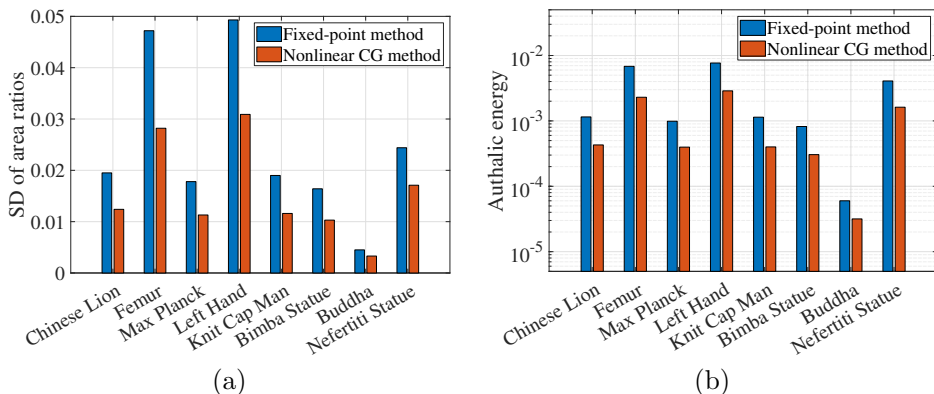


FIG. 5. The comparison of (a) SD of area ratios, defined in (5.1), and (b) the authalic energy, specified in (5.2), of the fixed-point method [25] and the nonlinear CG method (Algorithm 3.1).

From Table 1, we observe that the proposed nonlinear CG method, Algorithm 3.1, exhibits notably lower levels of local and global area distortions, along with improved computational efficiency, when compared to the fixed-point method [25].

The values of SDs of area ratios and authalic energies in Table 1 are visualized in Figure 5 (a) and (b), respectively. We observe that the maps computed by the proposed nonlinear CG method have significantly smaller values of SDs of area ratios and authalic energies than that of the fixed-point method, which indicates that the nonlinear CG method has better area-preserving accuracy.

Figure 6 further shows the relationship between numbers of vertices and the computational time cost of the fixed-point method [25] and the proposed nonlinear CG method, Algorithm 3.1. We observe that the efficiency of the proposed method for the SEM is significantly improved compared to the fixed-point method [25]. This improvement results in a computation time of less than 100 seconds for an area-preserving parameterization of a mesh with about 1 million vertices, which is reasonably satisfactory.

**6. Application to area-preserving surface registration.** In this section, we demonstrate a straightforward application of the proposed preconditioned CG method

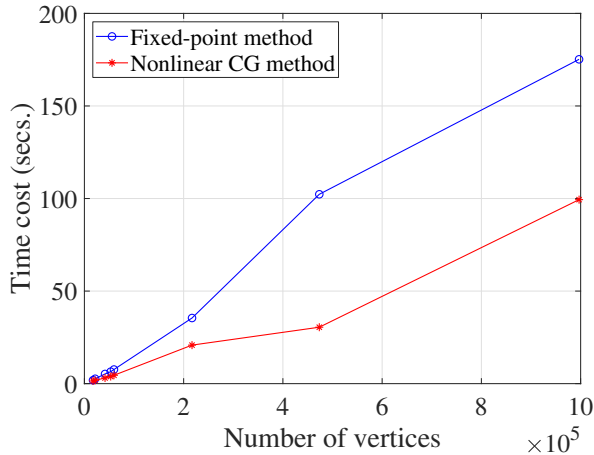


FIG. 6. The relationship between numbers of vertices and the computational time cost of the fixed-point method [25] and the proposed nonlinear CG method (Algorithm 3.1)

of SEM, Algorithm 3.1, for the registration task of surfaces. Surface registration is a widely studied problem in geometry processing [10, 13, 19, 25], but only a few studies have addressed surface registration with area-preserving properties.

In particular, we consider the registration task of two simply connected open surfaces  $\mathcal{S}$  and  $\mathcal{T}$  with landmark pairs  $\{(p_i, q_i) \mid p_i \in \mathcal{S}, q_i \in \mathcal{T}\}_{i=1}^m$ . The task aims to find a bijective mapping  $\varphi : \mathcal{S} \rightarrow \mathcal{T}$  that satisfies  $\varphi(p_i) \approx q_i$ , for  $i = 1, \dots, m$ . By applying the disk-shaped area-preserving parameterizations  $f : \mathcal{S} \rightarrow \mathbb{D}$  and  $g : \mathcal{T} \rightarrow \mathbb{D}$ , the registration task is simplified into finding a bijective mapping  $h : \mathbb{D} \rightarrow \mathbb{D}$  that satisfies  $h \circ f(p_i) \approx g(q_i)$ , for  $i = 1, \dots, m$ . Once we have such a map  $h$ , the registration mapping from  $\mathcal{S}$  to  $\mathcal{T}$  is constructed by  $\varphi = g^{-1} \circ h \circ f$ .

We suppose the triangular mesh  $\mathcal{S}$  consists of  $n$  vertices. The objective function for the registration task is formulated as a stretch energy with a penalty term given by

$$\tilde{E}_S(h) = E_S(h) + \lambda \sum_{i=1}^m \|h \circ f(p_i) - g(q_i)\|^2,$$

where  $\lambda$  is a positive real parameter. The gradient of  $\tilde{E}_S$  can be formulated as

$$\begin{aligned} \nabla \tilde{E}_S(h) &= 2 \left( (I_2 \otimes L_S(h)) \mathbf{h} + \lambda (I_2 \otimes P)^\top ((I_2 \otimes P) \mathbf{h} - \mathbf{g}) \right) \\ (6.1) \quad &= 2 \left( I_2 \otimes (L_S(h) + \lambda P^\top P) \right) \mathbf{h} - 2\lambda (I_2 \otimes P)^\top \mathbf{g}, \end{aligned}$$

where  $P$  is a permutation submatrix of size  $m$ -by- $n$  with

$$P_{i,j} = \begin{cases} 1 & \text{if the } i\text{th landmark of } \mathcal{S} \text{ is } j, \\ 0 & \text{otherwise.} \end{cases}$$

The minimizer of  $\tilde{E}_S$  satisfies  $\nabla \tilde{E}_S(h) = \mathbf{0}$ , i.e., the nonlinear system

$$(6.2) \quad (I_2 \otimes (L_S(h) + \lambda P^\top P)) \mathbf{h} = \lambda (I_2 \otimes P)^\top \mathbf{g}.$$

Under a prescribed boundary map  $\mathbf{h}_B = \mathbf{b}$ , the nonlinear system (6.2) becomes

$$(6.3) \quad [I_2 \otimes (L_S(h) + \lambda D)]_{I,I} \mathbf{h}_I = [\lambda (I_2 \otimes P)^\top \mathbf{g}]_I - [I_2 \otimes (L_S(h) + \lambda D)]_{I,B} \mathbf{b},$$

where  $D = P^\top P$  is a diagonal matrix with

$$D_{i,i} = \begin{cases} 1 & \text{if } i\text{th vertices is a landmark,} \\ 0 & \text{otherwise.} \end{cases}$$

The nonlinear system (6.3) can be solved by the fixed-point iteration

$$(6.4) \quad \left[ I_2 \otimes (L_S(h^{(k)}) + \lambda D) \right]_{\mathbf{I},\mathbf{I}} \mathbf{h}_{\mathbf{I}}^{(k+1)} = [\lambda(I_2 \otimes P)^\top \mathbf{g}]_{\mathbf{I}} - \left[ I_2 \otimes (L_S(h^{(k)}) + \lambda D) \right]_{\mathbf{I},\mathbf{B}} \mathbf{b},$$

with  $L_S(h^{(0)}) = L_S(\text{id})$ . To effectively solve the minimization problem

$$(6.5) \quad h = \underset{\mathbf{f}_{\mathbf{b}}=\mathbf{b}}{\operatorname{argmin}} \tilde{E}_S(f),$$

we apply Algorithm 3.1 by replacing the gradient direction with (6.1).

In practice, we demonstrate the registration mapping from the model Max Planck to Knit Cap Man. First, we compute area-preserving parameterizations  $f$  and  $g$  of Max Planck and Knit Cap Man surface models, respectively, using Algorithm 3.1. Then, we define feature curves of Max Planck and Knit Cap Man models on the disk-shaped parameter domains, as illustrated in Figure 7 (a) and (c). Next, we solve the minimization problem (6.5). The boundary map is chosen to be the optimal rotation with respect to the landmarks as

$$R = \underset{R \in SO(2)}{\operatorname{argmin}} \sum_{i=1}^m \|R(p_i) - q_i\|^2,$$

which can be solved by the singular value decomposition of a 2-by-2 matrix [17]. The initial map is computed by the fixed-point iteration (6.4) with 5 iteration steps. The computed registration mapping is presented in Figure 7 (b). It is worth noting that the map  $h$  is bijective with authalic energy  $E_A(h) = 5.04 \times 10^{-4}$ , and the positions of feature curves in Figure 7 (b) and (c) are identical up to an average error of  $10^{-3}$ , which means the registration mapping  $h$  preserves the area of the surface and keeps the specified facial features aligned well.

In Figure 8, we further show the linear homotopy  $\mathcal{H} : \mathbb{D} \times [0, 1] \rightarrow \mathbb{R}^3$  between the maps  $f^{-1}$  and  $g^{-1} \circ h$ , defined as

$$(6.6) \quad \mathcal{H}(v, t) = (1 - t) f^{-1}(v) + t (g^{-1} \circ h)(v).$$

We observe that the homotopy carried out by the registration map  $h$  effectively maintains the alignment of facial features of two surface models.

**7. Concluding remarks.** We have presented a new preconditioned nonlinear CG method of SEM for the computation of area-preserving parameterizations. The effectiveness of the proposed method is demonstrated to be significantly better than another state-of-the-art method in terms of area-preserving accuracy and computational efficiency. In addition, we have provided rigorous proof for the convergence of the proposed algorithm. Furthermore, a straightforward application of surface registration is presented. Such encouraging results make the SEM more valuable in practical computing area-preserving mappings.

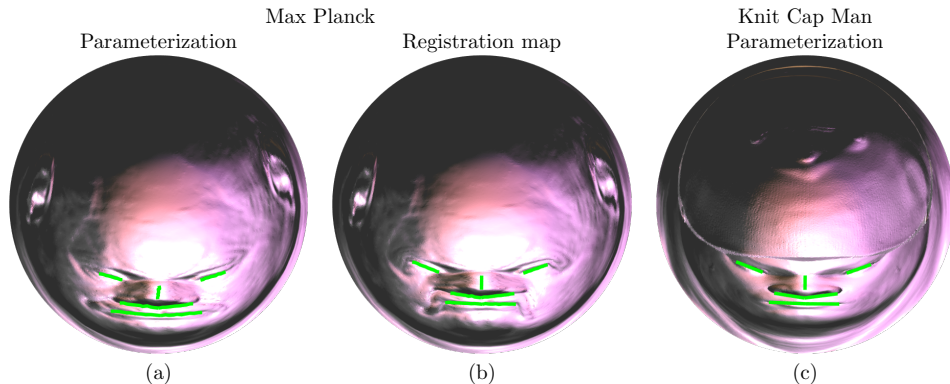


FIG. 7. The feature curves on the disk-shaped area-preserving parameter domains of (a) Max Planck and (c) Knit Cap Man, respectively, and (b) on the disk-shaped area-preserving registration map of Max Planck.

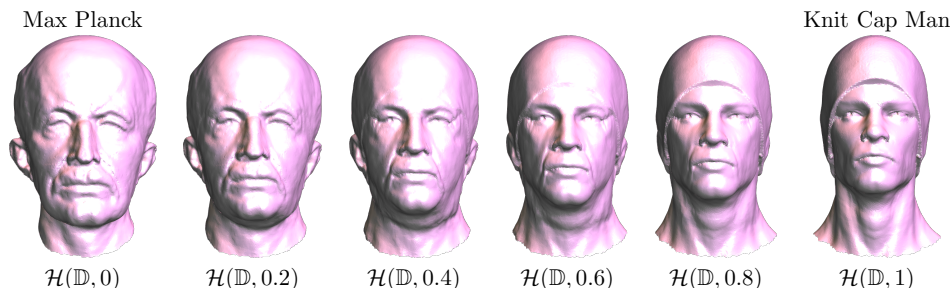


FIG. 8. The images of the linear homotopy (6.6) from Max Planck to Knit Cap Man.

## REFERENCES

- [1] *Digital Shape Workbench - Shape Repository*. <http://visionair.ge.imati.cnr.it/ontologies/shapes/>. (2016).
- [2] *The Stanford 3D Scanning Repository*. <http://graphics.stanford.edu/data/3Dscanrep/>. (2016).
- [3] *Sketchfab*. <https://sketchfab.com/>, (2019).
- [4] P. R. AMESTOY, T. A. DAVIS, AND I. S. DUFF, *Algorithm 837: AMD, an approximate minimum degree ordering algorithm*, *ACM Trans. Math. Softw.*, 30 (2004), pp. 381–388, <https://doi.org/10.1145/1024074.1024081>.
- [5] G. P. T. CHOI AND C. H. RYCROFT, *Density-equalizing maps for simply connected open surfaces*, *SIAM J. Imag. Sci.*, 11 (2018), pp. 1134–1178, <https://doi.org/10.1137/17M1124796>.
- [6] A. DOMINIZ AND A. TANNENBAUM, *Texture mapping via optimal mass transport*, *IEEE Trans. Vis. Comput. Graphics*, 16 (2010), pp. 419–433, <https://doi.org/10.1109/TVCG.2009.64>.
- [7] R. FLETCHER AND C. M. REEVES, *Function minimization by conjugate gradients*, *The Computer Journal*, 7 (1964), pp. 149–154.
- [8] M. S. FLOATER AND K. HORMANN, *Surface parameterization: a tutorial and survey*, in *Advances in Multiresolution for Geometric Modelling*, Springer Berlin Heidelberg, 2005, pp. 157–186, [https://doi.org/10.1007/3-540-26808-1\\_9](https://doi.org/10.1007/3-540-26808-1_9).
- [9] K. HORMANN, B. LÉVY, AND A. SHEFFER, *Mesh parameterization: Theory and practice*, in *ACM SIGGRAPH Course Notes*, 2007, <https://doi.org/10.1145/1281500.1281510>.
- [10] K. C. LAM AND L. M. LUI, *Landmark-and intensity-based registration with large deformations via quasi-conformal maps*, *SIAM J. Imag. Sci.*, 7 (2014), pp. 2364–2392.
- [11] W.-W. LIN, C. JUANG, M.-H. YUEH, T.-M. HUANG, T. LI, S. WANG, AND S.-T. YAU, *3D brain tumor segmentation using a two-stage optimal mass transport algorithm*, *Sci. Rep.*, 11 (2021), p. 14686.
- [12] W.-W. LIN, J.-W. LIN, T.-M. HUANG, T. LI, M.-H. YUEH, AND S.-T. YAU, *A novel 2-phase*

- residual U-net algorithm combined with optimal mass transportation for 3D brain tumor detection and segmentation*, Sci. Rep., 12 (2022), p. 6452.
- [13] L. M. LUI, K. C. LAM, S.-T. YAU, AND X. GU, *Teichmüller mapping (T-map) and its applications to landmark matching registration*, SIAM J. Imag. Sci., 7 (2014), pp. 391–426.
  - [14] J. NOCEDAL AND S. J. WRIGHT, *Numerical Optimization*, Springer, New York, NY, 2006.
  - [15] P. V. SANDER, J. SNYDER, S. J. GORTLER, AND H. HOPPE, *Texture mapping progressive meshes*, in Proceedings of the 28th Annual Conference on Computer Graphics and Interactive Techniques, SIGGRAPH '01, New York, NY, USA, 2001, ACM, pp. 409–416, <https://doi.org/10.1145/383259.383307>.
  - [16] A. SHEFFER, E. PRAUN, AND K. ROSE, *Mesh parameterization methods and their applications*, Found. Trends. Comp. Graphics and Vision., 2 (2006), pp. 105–171.
  - [17] O. SORKINE AND M. ALEXA, *As-rigid-as-possible surface modeling*, in Proceedings of EUROGRAPHICS/ACM SIGGRAPH Symposium on Geometry Processing, 2007, pp. 109–116.
  - [18] K. SU, L. CUI, K. QIAN, N. LEI, J. ZHANG, M. ZHANG, AND X. D. GU, *Area-preserving mesh parameterization for poly-annulus surfaces based on optimal mass transportation*, Comput. Aided Geom. D., 46 (2016), pp. 76 – 91, <https://doi.org/10.1016/j.cagd.2016.05.005>.
  - [19] Y. YOSHIYASU, W.-C. MA, E. YOSHIDA, AND F. KANEHIRO, *As-conformal-as-possible surface registration*, in Comput. Graph. Forum, vol. 33, Wiley Online Library, 2014, pp. 257–267, <https://doi.org/10.1111/cgf.12451>.
  - [20] S. YOSHIKAWA, A. BELYAEV, AND H. P. SEIDEL, *A fast and simple stretch-minimizing mesh parameterization*, in Proceedings Shape Modeling Applications, 2004., June 2004, pp. 200–208, <https://doi.org/10.1109/SML.2004.1314507>.
  - [21] M.-H. YUEH, *Theoretical foundation of the stretch energy minimization for area-preserving simplicial mappings*, arXiv:2205.14414 (2022), <https://doi.org/10.48550/ARXIV.2205.14414>. (accepted for publication in *SIAM J. Imaging Sci.*).
  - [22] M.-H. YUEH, T. LI, W.-W. LIN, AND S.-T. YAU, *A novel algorithm for volume-preserving parameterizations of 3-manifolds*, SIAM J. Imag. Sci., 12 (2019), pp. 1071–1098, <https://doi.org/10.1137/18M1201184>.
  - [23] M.-H. YUEH, T. LI, W.-W. LIN, AND S.-T. YAU, *A new efficient algorithm for volume-preserving parameterizations of genus-one 3-manifolds*, SIAM J. Imag. Sci., 13 (2020), pp. 1536–1564.
  - [24] M.-H. YUEH, W.-W. LIN, C.-T. WU, AND S.-T. YAU, *An efficient energy minimization for conformal parameterizations*, J. Sci. Comput., 73 (2017), pp. 203–227, <https://doi.org/10.1007/s10915-017-0414-y>.
  - [25] M.-H. YUEH, W.-W. LIN, C.-T. WU, AND S.-T. YAU, *A novel stretch energy minimization algorithm for equiareal parameterizations*, J. Sci. Comput., 78 (2019), pp. 1353–1386, <https://doi.org/10.1007/s10915-018-0822-7>.
  - [26] X. ZHAO, Z. SU, X. D. GU, A. KAUFMAN, J. SUN, J. GAO, AND F. LUO, *Area-preservation mapping using optimal mass transport*, IEEE Trans. Vis. Comput. Gr., 19 (2013), pp. 2838–2847, <https://doi.org/10.1109/TVCG.2013.135>.
  - [27] G. ZOU, J. HU, X. GU, AND J. HUA, *Authalic parameterization of general surfaces using Lie advection*, IEEE Trans. Vis. Comput. Graph., 17 (2011), pp. 2005–2014, <https://doi.org/10.1109/TVCG.2011.171>.